ACS OMEGA

http://pubs.acs.org/journal/acsodf

Article

Isoflavonoid and Furanochromone Natural Products as Potential DNA Gyrase Inhibitors: Computational, Spectral, and Antimycobacterial Studies

Vilas R. Jagatap, Iqrar Ahmad, Dharmarajan Sriram, Jyothi Kumari, Darko Kwabena Adu, Blessing Wisdom Ike, Meenu Ghai, Siddique Akber Ansari, Irfan Aamer Ansari, Priscille Ornella Mefotso Wetchoua, Rajshekhar Karpoormath, and Harun Patel*

Cite This: *ACS Omega* 2023, 8, 16228−16240

Read Online

ACCESS | Metrics & More | Article Recommendations | Supporting Information

ABSTRACT: In pursuit of new antitubercular agents, we here report the antimycobacterial ($H_{37}Rv$) and DNA gyrase inhibitory potential of daidzein and khellin natural products (NPs). We procured a total of 16 NPs based on their pharmacophoric similarities with known antimycobacterial compounds. The $H_{37}Rv$ strain of *M. tuberculosis* was found to be susceptible to only two out of the 16 NPs procured; specifically, daidzein and khellin each exhibited an MIC of 25 μg/mL. Moreover, daidzein and khellin inhibited the DNA gyrase enzyme with IC_{50} values of 0.042 and 0.822 μg/mL, respectively, compared to ciprofloxacin with an IC_{50} value of 0.018 μg/mL. Daidzein and khellin were found to have lower toxicity toward the vero cell line, with IC_{50} values of 160.81 and 300.23 μg/mL, respectively. Further, molecular docking study and MD simulation of daidzein indicated that it remained stable inside the cavity of DNA GyrB domain for 100 ns.

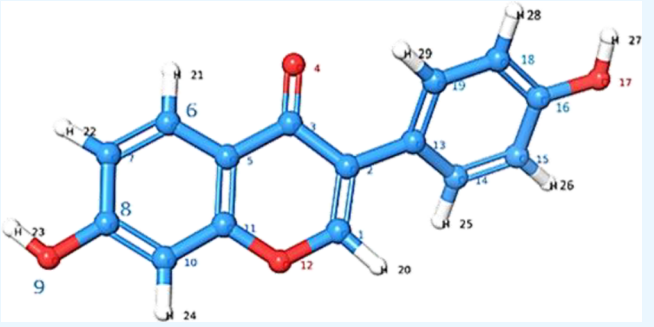

1. INTRODUCTION

Tuberculosis (TB) is a serious, fatal, communicable, infectious, and pandemic illness caused by *M. tuberculosis*, *M. africanum*, *M. bovis*, *M. laprae*, *M. avium*, and *M. microti*.[1−9] The WHO has published its data on tuberculosis fatalities, revealing that 1.5 million individuals died from the disease in 2020, which included 214,000 individuals living with HIV.[10] Besides COVID-19 and HIV/AIDS, TB is the 13th leading global cause of death and the 2nd most common infectious killer in the world.[10−14] With 3.3 million women, 5.6 million men, and 1.1 million children among those afflicted, it is predicted that 10 million new cases of TB would be reported globally in 2020.[10]

The 30 countries with the highest TB burden will account for 86% of new TB infections in 2020. Two-thirds of the cases are from eight nations, with India leading the way, followed by "*China, Indonesia, the Philippines, Pakistan, Nigeria, Bangladesh, and South Africa*".[10] The rate of tuberculosis in the world is falling at a rate of about 2% per year, and between 2015 and 2020, it fell by 11%.[10]

Unfortunately, *M. tuberculosis* is resistant to nearly all first- and second-line anti-TB medications, resulting in drug-resistant tuberculosis, a major public health concern.[15] Plants have been shown to be a significant source of bioactive substances, and over 75% of all antibacterial chemicals are from natural sources.[16] Natural products (NPs) are multitarget molecules that may minimize drug resistance; to date, various natural metabolites have been evaluated for antimycobacterial efficacy.[17,18]

Natural substances have always piqued the interest of medical chemists due to their numerous medicinal properties. Even today, it is estimated that 60% of the world's population relies on biologically active plants for primary healthcare.[19] Among the phytocompounds, isoflavonoids and chromones are well known for their antimycobacterial activity. Coronado-Aceves et al. extracted precatorin C isoflavonoid from the extract of *Rhynchosia precatoria*, and it displayed an MIC of 62.5 μg/mL against the $H_{37}Rv$ strain.[20] Songsiang et al. in another study separated the dalparvone isoflavonoid from the stem part of *Dalbergia parviflora*, and it showed significant anti-TB potential with an MIC of 50 μg /mL (Figure 1).[21] Chokchaisiri and researchers extracted isoflavonoid NPs like formononetin, afromosin, and formononetin-7-*O*-D-glucopyr-

Received: February 2, 2023
Accepted: April 18, 2023
Published: April 28, 2023

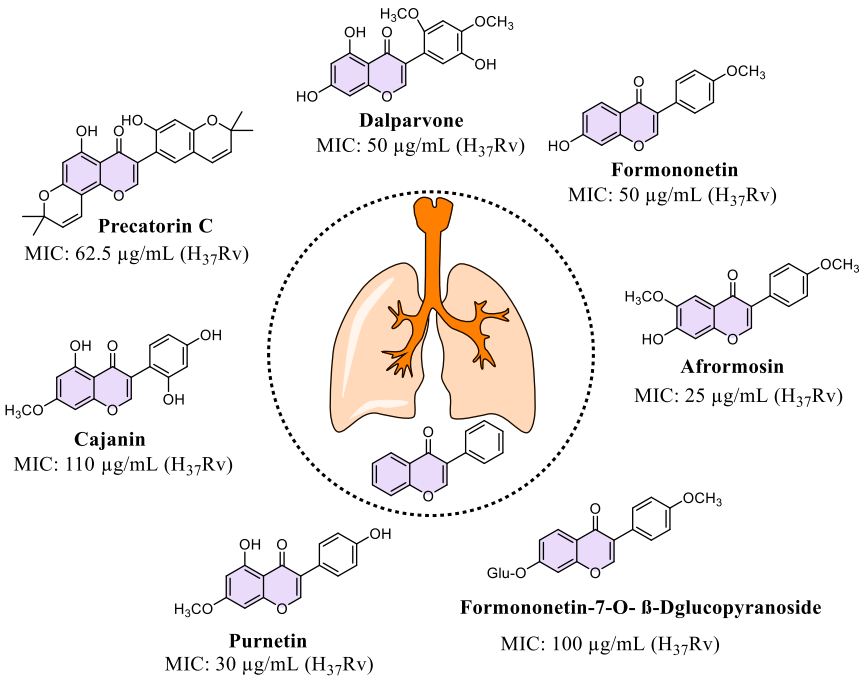

Figure 1. Isoflavonoid containing NPs with their antimycobacterial potential.

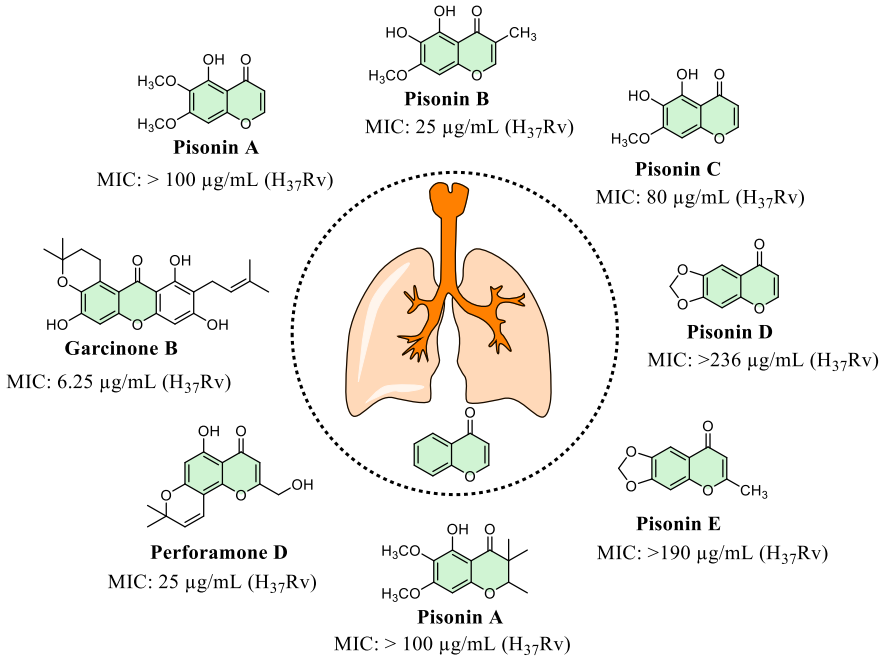

Figure 2. Chromone-containing NPs with antimycobacterial potential.

anoside from *Butea monosperma* flowers. For extraction, they used *n*-hexane and methanol as solvents. The team further investigated the antimycobacterial potential of the isolated NPs, and they found that all extracted plant constituents were active against mycobacteria with MICs of 50 μg/mL, 25 μg/mL, and 100 μg/mL (Figure 1).[22] Chen et al. isolated prunetin and cajanin isoflavonoids from the root of *Ficus nervosa* with MICs of 30 μg/mL and 110 μg/mL against *M. tuberculosis* $H_{37}Rv$, respectively (Figure 1).[23]

Like the isoflavonoids, chromones have also been reported for their antimycobacterial potential.

Wu et al. isolated pisonin A, B, C, D, and E (chromones) from the methanolic extract of *Pisonia aculeata* stem and root and tested them for antimycobacterial activity. Pisonin B was discovered to have remarkable antimycobacterial activity, with an MIC of 25 μg/mL (Figure 2).[24]

Tuntiwachwuttikul et al. extracted four new chromones, namely, perforamone A, B, C, and D, from the branches of *Harrisonia perforata*, along with six recognized phyto-chemicals like perforatic acid, *O*-methylalloptaeroxylin, peucenin-7-methyl ether, eugenin, greveichromenol, and saikochromone A. Perforamone D was the most active chromone-containing isolate with an MIC of 25 μg/mL toward the $H_{37}Rv$ (Figure

https://doi.org/10.1021/acsomega.3c00684
ACS Omega 2023, 8, 16228−16240

2).[25] Skusamrarn and coauthors isolated bioactive NPs from the fruit hulls of *Garcinia mangostana*.[26] Among the isolated bioactives, garcinone B was the most active isolate toward the *Mtb* H_{37}Rv strain with an MIC of 6.25 μg/mL. Considering the antimycobacterial potential of natural products, we herein report the antimycobacterial study of the NP containing the isoflavonoid, chromone, coumarin, chalcones, anthraquinone, pyrimidine, quinoline, piperidine, and piperazine core and further molecular mechanistic study of the potent compounds to validate the drug target.

2. RESULTS AND DISCUSSION

2.1. Procurement of NPs. A total of 16 pure NPs were procured from Yucca enterprises, Antop Hill, Wadala East, Mumbai, India. The selection of NPs was based on their shared pharmacophore features with reported antimycobacterial compounds such as flavonoid,[27] isoflavonoid,[27] chromone,[24] coumarin,[28] chalcone,[29] anthraquinone,[30] pyridine,[31] quinoline,[32] piperidine, and piperazine.[33] The certificate of analysis (COA) and percentage purity data of purchased NPs are attached in the supplementary information file, and the details are given in Table 1.

Table 1. Percent (%) Purity of the Procured NPs

sr. no	name of natural product	percent (%) purity
1	Thaumatin B	96%
2	Quinine sulfate	99%
3	Gmelinol	95.2%
4	Nicotine bi-L-(+)-tartarate dihydrate	99.6%
5	Lobeline hydrochloride	>98%
6	Diacerein	99%
7	Chlorogenic acid	98%
8	Flavokawain A	>98%
9	Diosmin	96.2%
10	Neohesperidin	95%
11	Paeoniflorin	97%
12	Dihydromyricetin	96%
13	Chrysin	>98%
14	Aesculin	>98%
15	Daidzein	>98%
16	Khellin	98.6%

2.2. Physical and Spectral Characterization of the Potent NPs. *2.2.1. Daidzein.* R_f: 0.70 in benzene: acetone (6:4 ratio); mp: 322−324 °C; IR ν_{max} (KBr pellets): 3158.57 (OH Stretch), 2823.79 (CH Stretch), 1674.21 (C═O) cm^{-1}; ^{1}H NMR (500 MHz, DMSO-d_6): δ 10.81 (s, 1H, OH, 7-OH chromen-4-one), 9.56 (s, 1H, 4-OH phenyl), 8.29 (s, 1H, chromen-4-one ring), 7.9594−7.9769 (d, 1H, chromen-4-one ring), 7.3686−7.3972 (notched doublet, 2H, Phenyl), 6.9272−6.9492 (notched doublet, 1H, chromen-4-one ring), 6.7947−6.8233 (Notched doublet, 2H, Phenyl), 6.8649 (s, 1H, chromen-4-one ring) ppm; ^{13}C NMR (DMSO-d_6) 174.56 (C═O), 162.38,157.30, 157.05, 152.69, 129.94, 127.16, 123.36, 122.42, 116.51, 115.00, 114.82, 101.97 (Ar−C) ppm; MS (ES+): 255.2 $[M + H]^+$ (Supplementary Information, Figures S1−S4).

2.2.2. Khellin. R_f: 0.58 in benzene: acetone (7:3 ratio); mp: 154−156 °C; IR ν_{max} (KBr pellets): 3097.68 (Aro. CH Stretch), 2935.66 (Ali. CH Stretch) 1668.23 (C═O) cm^{-1}; ^{1}H NMR (500 MHz, DMSO-d_6): δ 8.1039−8.1084 (d, 1H, furan ring), 7.2252−7.2298 (d, 1H, furan ring), 6.0779 (s, 1H, chromen-4-one ring), 4.1039 (s, 3H, OCH_3), 3.9313 (s, 3H, OCH_3), 2.3759 (s, 3H, CH_3); ^{13}C NMR (DMSO-d_6) 176.51 (C═O), 164.15, 148.17, 146.91, 146.59, 129.25, 118.77, 113.05, 109.88, 105.33 (Ar−C), 61.68 (OCH_3), 61.11 (OCH_3), 19 (CH_3) ppm; MS (ES+): 261.2 $[M + H]^+$ (Supplementary Information, Figures S5−S9).

2.3. Antimycobacterial Activity. The total of 16 NPs (Figure 3) were procured from Yucca Enterprises, Antop hill, Wadala East, Mumbai. The choice of phytomolecules was made based on their shared pharmacophore features with the reported antimycobacterial compounds.[24,27−33] Using the MABA assay protocol, these compounds were tested for antimycobacterial activity against the H_{37}Rv strain. Among the screened compounds, daidzein and khellin were found to be effective against the mycobacterial strain with an MIC value of 25 μg/mL as compared to isoniazid, rifampicin, and ethambutol, which were used as standard antitubercular drugs (Figure 3). On the other hand, the remaining 14 phytocompounds, namely, thaumatin B, quinine sulfate, gmelinol, nicotine bi-L-(+)-tartarate dihydrate, lobeline hydrochloride, diacerein, chlorogenic acid, flavokawain A, diosmin, neohesperidin, paeoniflorin, dihydromyricetin, chrysin, and aesculin were moderately active with an MIC value of >25 μg/mL. Further, "*structure activity relationship*" revealed that the chromene scaffold containing NPs (daidzein and khellin) were more active than the chroman scaffold (paeoniflorin, neohesperidin, and dihydromyricetin). Among the chromenes, chromen-4-one (daidzein) and chromen-5-one (khellin) were more potent than the chromen-2-one (aesculin) (Figure 3). The cytotoxic concentration of daidzein and khellin was found to be 160.81 μg/mL and 300.23 μg/mL, respectively, against the vero cell line (Figure 3).

2.4. DNA Gyrase Activity. Daidzein and khellin were biologically evaluated for their ability to inhibit activity associated with *E. coli* DNA gyrase *in vitro* using the DNA supercoiling assay kit (TopoGen) as mentioned in the methods section. All reactions were carried out on the *E. coli* DNA gyrase enzyme using three different concentrations of the compounds. The positive control (relaxed pBR322 DNA+ DNA gyrase enzyme) showed a supercoiled DNA band, whereas the negative control (relaxed pBR322 DNA without the DNA gyrase enzyme) displayed a relaxed DNA band. The gel assay showed that both daidzein and khellin showed significant DNA gyrase inhibition with IC_{50} values of 0.042 μg/mL and 0.822 μg/mL, respectively, compared to ciprofloxacin with an IC_{50} value of 0.018 μg/mL.

2.5. Docking Study. The active phytocompounds, namely, daidzein and khellin, were docked in the DNA GyrB domain of *M. tuberculosis* obtained from the "*protein data bank*" (PDB ID: 5BS8). For antimycobacterial drugs, DNA gyrase is one of the most important targets.[34] DNA gyrase (topoisomerase II), an ATP-dependent enzyme involved in "*DNA replication, transcription, and chromosome segregation*", is a tetrameric enzyme composed of two A and two B subunits, which are, respectively, encoded by the genes gyrA and gyrB.[35] The A subunit is required for the breakage and reunification of DNA double strands, while the B subunit is required for the energy-transfer process involving ATP hydrolysis.[34,35] The "*molecular docking and binding free energy*" calculations were performed to study molecular interactions between promising compounds daidzein and khellin and the binding site of *Mtb* DNA GyrB (PDB ID: 5BS8). The protein was first processed with Schrödinger Suite 2012s Protein Preparation Wizard. There

https://doi.org/10.1021/acsomega.3c00684
ACS Omega 2023, 8, 16228−16240

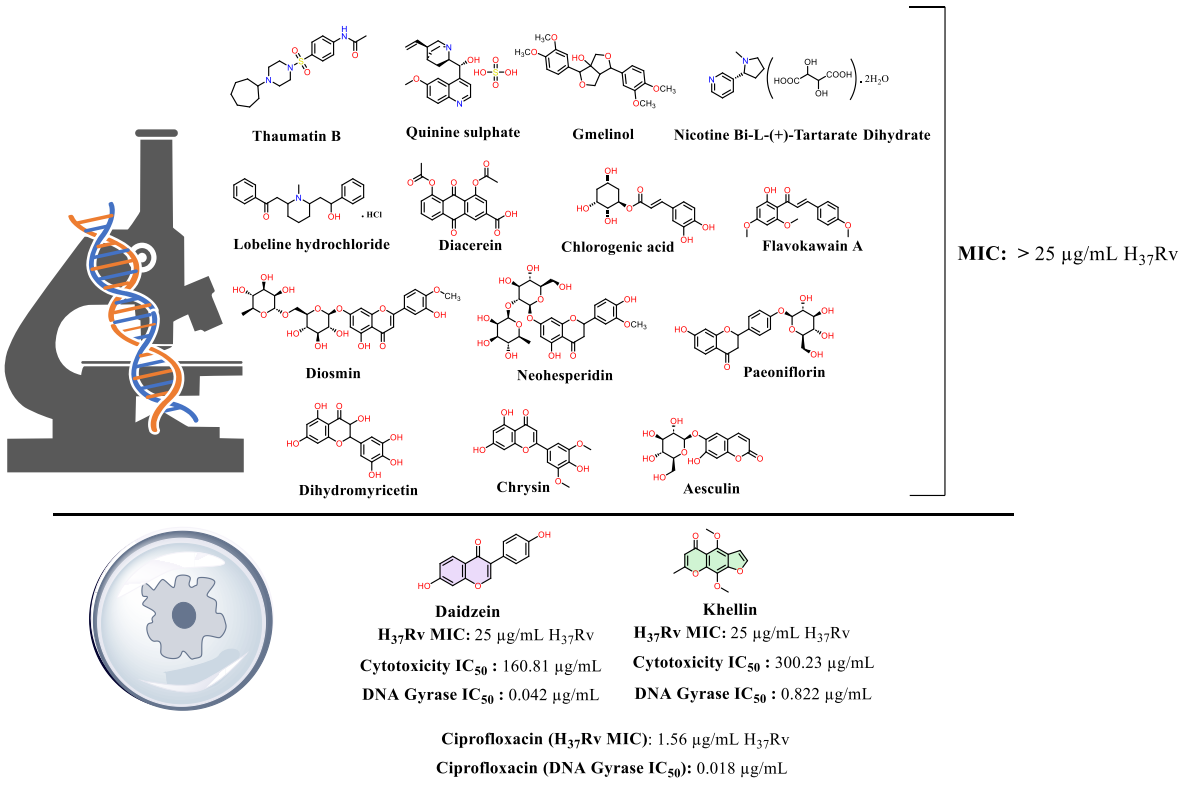

Figure 3. *In vitro* antimycobacterial and DNA gyrase inhibitory potential of the NPs.

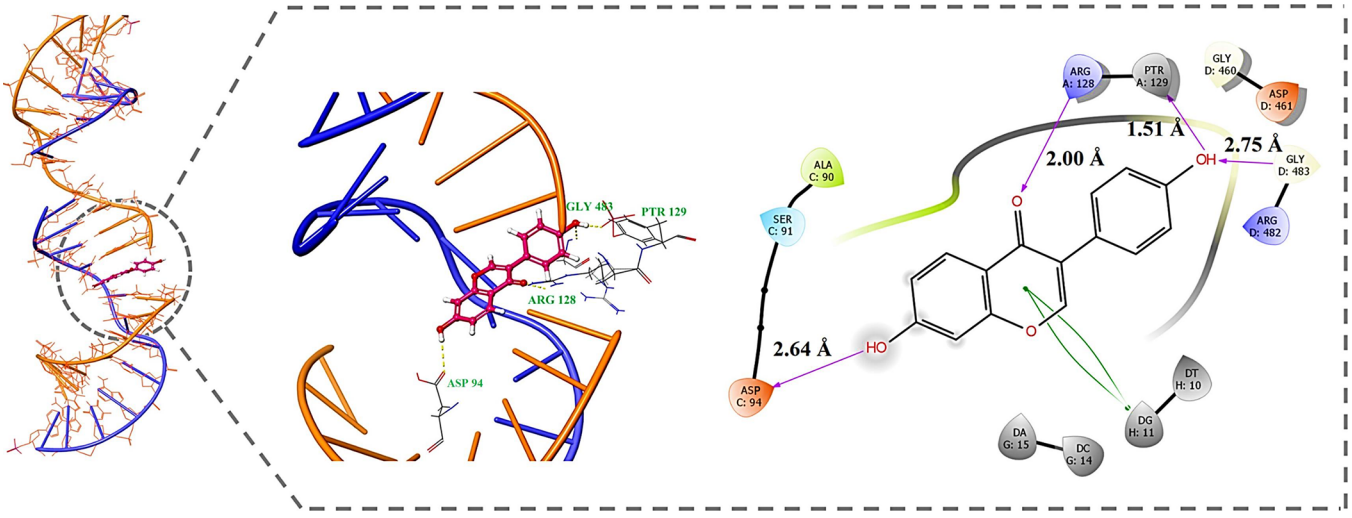

Figure 4. 3D and 2D interactions of daidzein with DNA GyrB.

Table 2. Docking Study and Binding Free Energy Calculations of the NPs toward the *Mtb* DNA Gyrase

compounds	docking score	glide ligand efficiency	glide gscore	glide lipo	glide rewards	glide evdw	glide ecoul	glide emodel	glide energy
Daidzein	−7.449	−0.392	−7.457	−1.985	−1.676	−33.83	−13.942	−70.257	−47.772
Khellin	−6.992	−0.368	−6.992	−2.873	−1.635	−37.967	−2.267	−57.768	−40.234
Ciprofloxacin	−9.467	−0.394	−9.567	−3.829	−2.307	−46.025	−7.022	−89.711	−53.047
binding free energy by MMGBSA									
compounds	MMGBSA ΔG bind	MMGBSA ΔG bind coulomb	MMGBSA ΔG bind covalent	MMGBSA ΔG bind Hbond	MMGBSA ΔG bind lipo	MMGBSA ΔG bind packing	MMGBSA ΔG bind solv GB	MMGBSA ΔG bind vdW	
daidzein	−42.75	−23.15	2.39	−2.34	−7.81	−6.31	32.84	−38.37	
khellin	−42.24	−12.35	0.21	−1.69	−6.4	−11.58	29.23	−39.65	
ciprofloxacin	−44.24	133.00	1.63	−1.96	−9.89	−6.80	−105.96	−54.86	

https://doi.org/10.1021/acsomega.3c00684
ACS Omega 2023, 8, 16228−16240

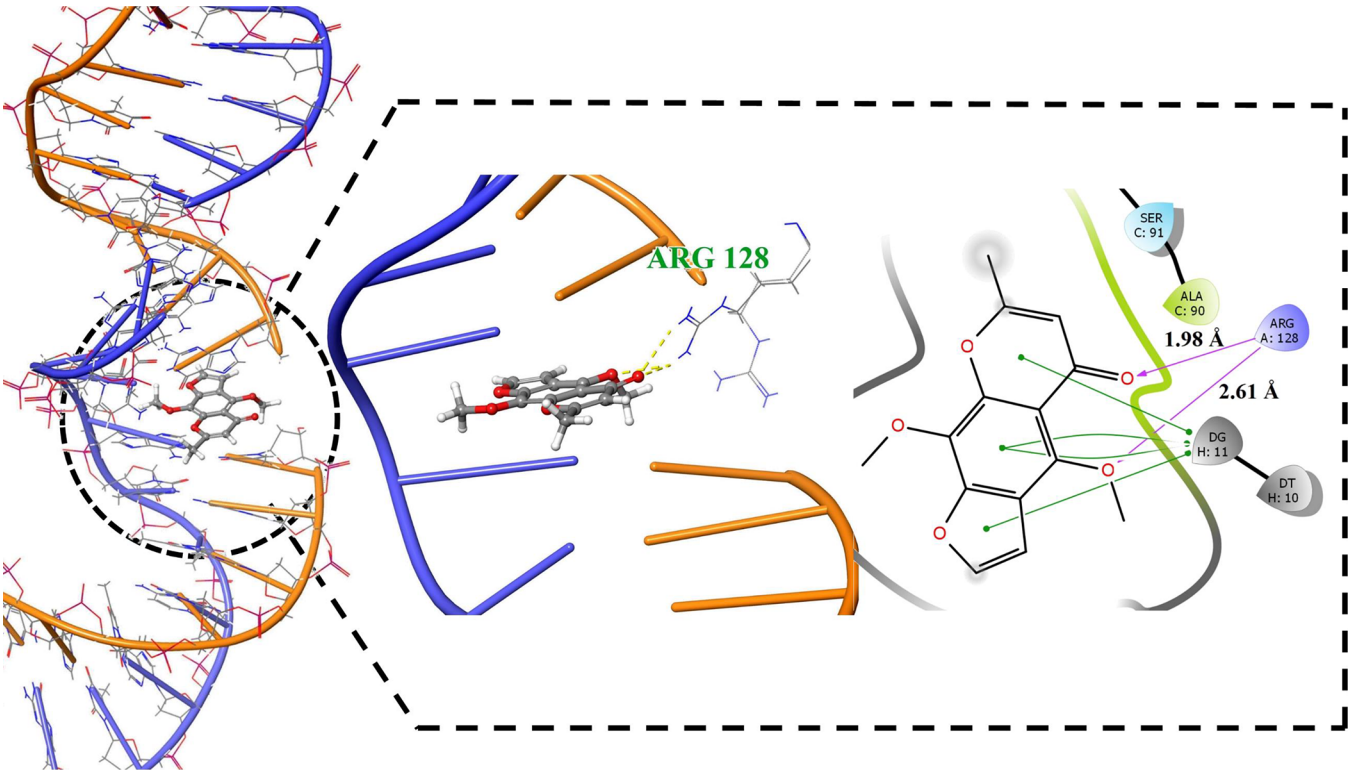

Figure 5. 3D and 2D interactions of khellin with DNA GyrB.

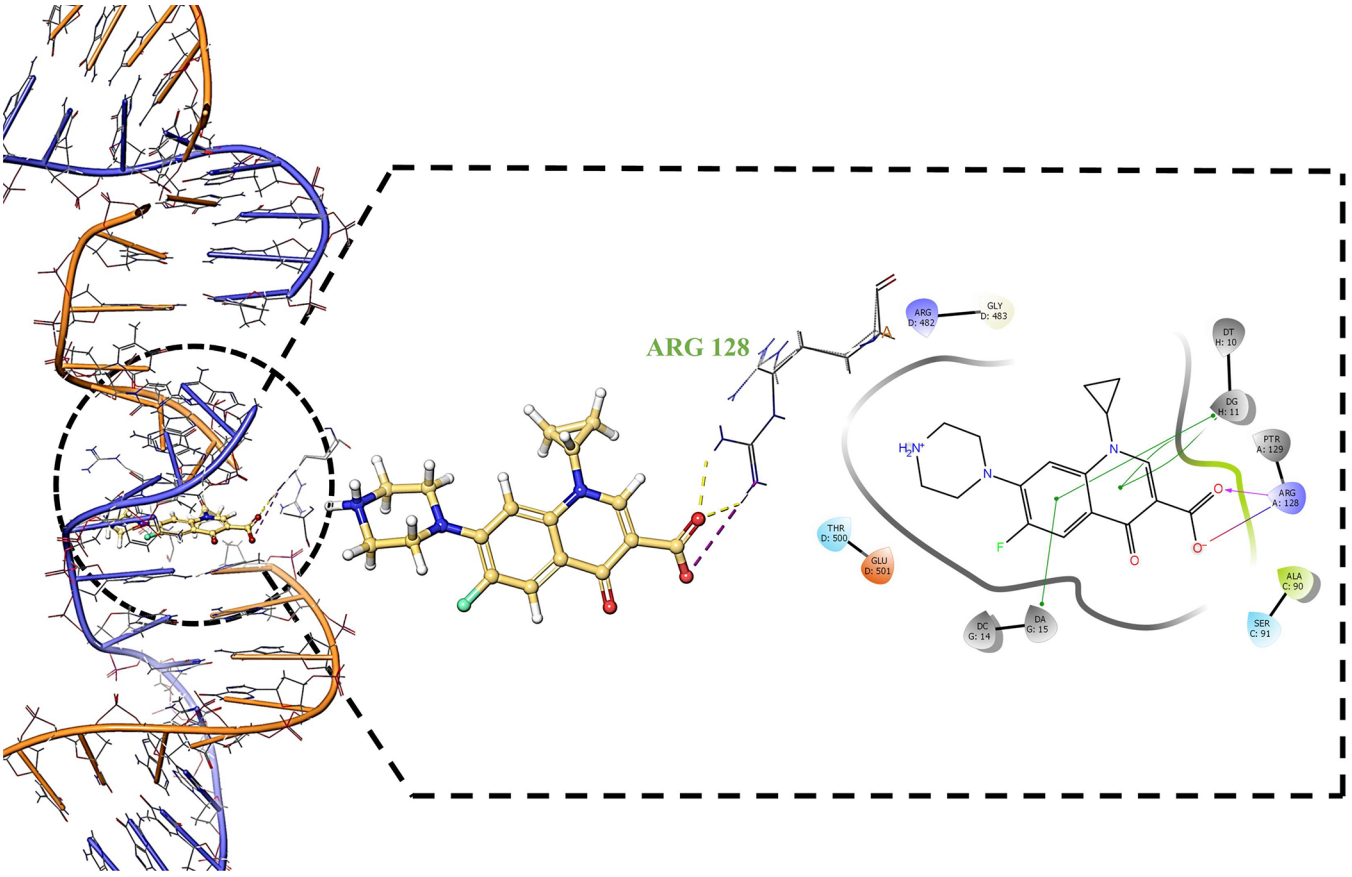

Figure 6. 3D and 2D interactions of ciprofloxacin with DNA GyrB.

was overlap between the EF and GH chains (both are DNA double-helical strands). Hence, we reserved the GH chain containing the co-crystallized ligand and deleted the EF. The protein and ligands were optimized using the "*OPLS force*

https://doi.org/10.1021/acsomega.3c00684
ACS Omega 2023, 8, 16228−16240

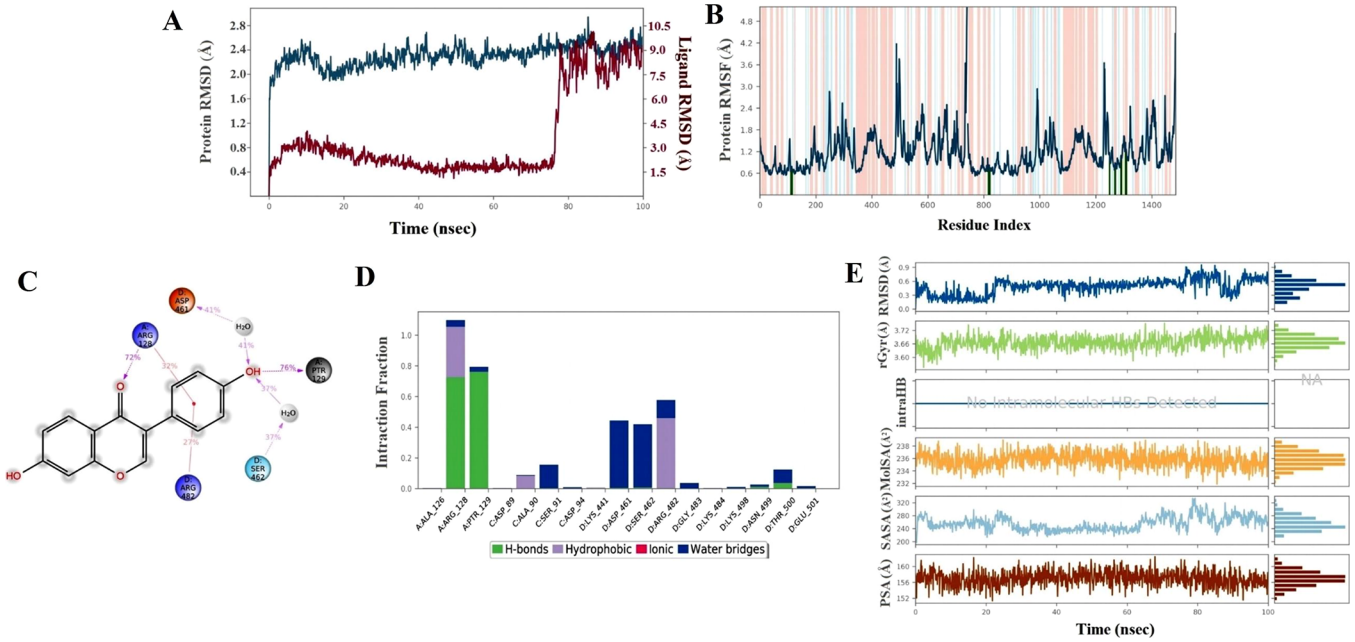

Figure 7. Molecular dynamic simulation profile of daidzein. (A) RMSD of the ligand (daidzein) and protein (GyrB) in bound form; (B) RMSF of GyrB during 100 ns; (C,D) interaction profile of daidzein with GyrB; (E) ligand (daidzein) properties during 100 ns of MD simulation.

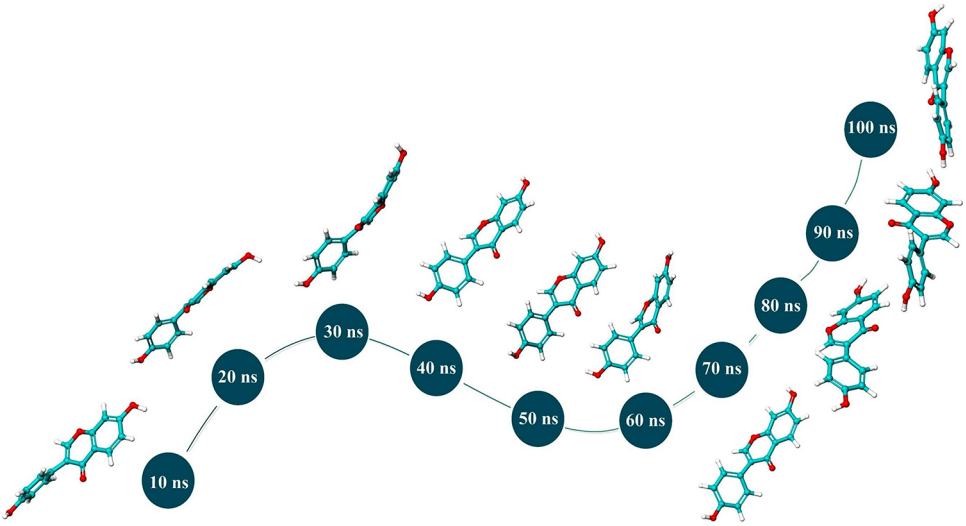

Figure 8. Different conformations of daidzein during 100 ns of simulation.

field". The grid was generated around the co-crystallized ligand moxifloxacin.

The docking interaction analysis for active analogues daidzein and khellin revealed that the molecules were lodged in the active site via hydrogen bond interaction and hydrophobic interaction. A docking study indicated that daidzein (−7.449 kcal/mol) had a higher binding affinity with a DNA GyrB domain followed by khellin (−6.992 kcal/mol) compared to ciprofloxacin (−9.467 kcal/mol). Daidzein formed hydrogen bond interactions via the 7-hydroxy group present on chromen-4-one of daidzein. The carbonyl oxygen at the C-4 position of the chromen-4-one ring established the hydrogen bond interaction with Arg 128 (similar to the cocrystallized ligand ciprofloxacin). The chromen-4-one ring interacted with the DG H:11 nucleotide of the DNA via $\pi-\pi$ stacking interaction. The 4-hydroxy group of 4-hydroxyphenyl formed two hydrogen bond interactions, one with Gly 483 and the other with PTR (phosphonotyrosine) 129 (Figure 4 and Table 2).

Khellin showed two hydrogen bond interactions via the carbonyl oxygen and methoxy oxygen of the furanochromone ring with Arg 128 amino acid (like ciprofloxacin). The furanochromone ring of khellin itself was involved in the $\pi-\pi$ interaction with the DG:11 nucleotide of the DNA (Figure 5 and Table 2).

Ciprofloxacin formed a hydrogen bond interaction and salt bridge interaction *via* carboxylic acid group at the C-3 position of the quinoline ring with Arg 128 amino acid. The quinoline ring itself established the $\pi-\pi$ interaction with the DA:15 and DG:11 nucleotides of the DNA (Figure 6 and Table 2). Binding free energy analysis indicated that daidzein (−42.75 kcal/mol) and khellin (−42.24 kcal/mol) were having comparative binding free energy score compared to ciprofloxacin (−44.24 kcal/mol) (Table 2).

https://doi.org/10.1021/acsomega.3c00684
ACS Omega 2023, 8, 16228−16240

Table 3. MMGBSA (Binding Free Energy) Calculation of Daidzein during 100 ns Time of Simulation

nano second time of simulation	MMGBSA ΔG bind	MMGBSA ΔG bind coulomb	MMGBSA ΔG bind covalent	MMGBSA ΔG bind lipo	MMGBSA ΔG bind solv	MMGBSA ΔG bind vdW
0	−131.16	−157.20	16.58	−11.85	128.00	−106.62
1	−169.25	−795.46	8.07	−13.19	765.91	−134.36
2	−158.76	−680.96	9.48	−12.53	665.14	−139.89
3	−198.04	−698.96	11.78	−14.43	640.94	−136.01
4	−166.66	−694.32	15.49	−14.47	663.13	−136.48
5	−170.04	−444.94	16.85	−13.95	407.46	−135.45
6	−132.84	−270.17	10.54	−11.15	260.39	−122.44
7	−138.96	281.93	8.18	−14.03	−264.44	−150.60
8	−122.10	335.55	24.37	−16.28	−298.73	−165.96
9	−131.56	297.83	20.82	−16.24	−273.01	−160.13
10	−124.34	220.53	22.77	−19.01	−186.18	−161.08
11	−134.36	312.84	11.39	−15.50	−280.73	−160.83
12	−133.44	−43.24	19.86	−15.61	58.85	−152.14
13	−136.00	69.20	22.08	−16.24	−51.57	−157.96
14	−124.69	346.95	27.22	−16.00	−335.78	−145.24
15	−153.53	−446.87	19.65	−16.71	437.92	−146.68
16	−135.94	−121.97	10.66	−14.04	148.03	−157.19
17	−107.12	393.40	19.52	−15.57	−351.39	−151.23
18	−135.34	278.37	21.20	−15.87	−262.19	−155.25
19	−134.61	198.01	19.32	−16.51	−180.85	−153.01
20	−116.00	427.82	12.28	−17.79	−380.96	−155.67
21	−176.51	−660.51	16.01	−18.08	641.45	−153.70
22	−177.13	−544.83	14.04	−14.12	508.35	−140.55
23	−153.03	−49.88	19.91	−16.34	66.80	−171.95
24	−161.46	−564.51	22.88	−15.62	551.92	−154.84
25	−182.28	−754.07	16.42	−13.73	724.96	−154.17
26	−183.34	−677.22	13.04	−14.84	643.13	−145.89
27	−167.85	−691.28	20.17	−15.41	678.31	−158.25
28	−182.90	−730.25	17.59	−13.73	690.15	−144.87
29	−153.21	−223.17	23.21	−14.40	201.95	−140.00
30	−143.10	71.32	15.21	−14.17	−53.46	−160.43
31	−138.18	144.99	24.01	−15.56	−135.95	−153.68
32	−107.23	602.13	21.56	−14.93	−569.18	−145.00
33	−195.74	−542.96	12.88	−15.75	512.28	−160.38
34	−208.15	−875.66	12.74	−13.91	815.23	−144.66
35	−189.49	−729.50	19.72	−15.88	697.34	−159.65
36	−159.97	−439.03	25.91	−16.42	421.17	−150.04
37	−123.95	119.20	24.38	−14.10	−93.45	−158.26
38	−152.60	−474.52	23.63	−16.32	470.66	−155.49
39	−174.58	−532.36	27.87	−14.76	490.85	−144.96
40	−184.20	−362.98	12.16	−14.32	332.06	−150.08
41	−172.15	−420.34	17.09	−16.19	410.20	−161.77
42	−119.60	190.00	13.40	−13.27	−163.23	−145.36
43	−118.98	370.31	16.81	−14.30	−342.73	−148.09
44	−107.14	473.55	25.94	−18.01	−427.45	−160.02
45	−168.19	−187.91	9.67	−15.10	177.01	−150.90
46	−129.65	−201.84	10.98	−17.21	232.69	−153.62
47	−174.38	−566.82	20.00	−15.46	534.43	−145.82
48	−182.47	−676.45	12.64	−14.23	647.16	−150.40
49	−199.75	−783.99	13.27	−17.33	745.47	−156.25
50	−149.18	352.62	12.33	−15.97	−340.23	−156.82
51	−168.79	−415.28	8.98	−15.20	401.08	−147.33
52	−147.28	154.37	14.25	−12.81	−160.54	−142.44
53	−128.80	−192.90	22.79	−16.48	205.20	−146.80
54	−168.25	−262.44	15.50	−16.43	245.76	−149.46
55	−142.40	−2.87	5.47	−12.39	6.02	−137.29
56	−137.56	−141.47	11.68	−13.36	153.03	−146.20
57	−128.50	−424.36	13.57	−13.30	450.04	−153.30
58	−168.15	−603.90	5.64	−15.37	590.80	−144.04
59	−146.20	38.81	16.45	−15.66	−30.40	−154.72

https://doi.org/10.1021/acsomega.3c00684
ACS Omega 2023, 8, 16228−16240

Table 3. continued

nano second time of simulation	MMGBSA ΔG bind	MMGBSA ΔG bind coulomb	MMGBSA ΔG bind covalent	MMGBSA ΔG bind lipo	MMGBSA ΔG bind solv	MMGBSA ΔG bind vdW
60	−121.85	339.34	0.70	−14.21	−307.43	−139.06
61	−119.77	409.26	14.51	−12.44	−372.52	−157.29
62	−113.11	527.78	25.91	−15.19	−497.32	−152.99
63	−158.97	−615.51	19.78	−14.26	591.53	−139.43
64	−141.57	−261.32	11.49	−14.59	262.87	−140.01
65	−155.23	137.09	10.45	−16.32	−140.13	−145.66
66	−181.75	−221.29	14.33	−16.30	190.76	−148.10
67	−157.31	−90.27	9.83	−16.13	78.45	−138.84
68	−121.90	426.04	17.80	−16.93	−415.30	−132.71
69	−179.35	−362.24	10.33	−15.35	325.61	−136.81
70	−193.85	−825.69	17.49	−16.75	777.72	−145.65
71	−154.84	−286.77	17.79	−15.77	257.82	−126.94
72	−186.44	−657.95	14.65	−14.61	610.58	−138.42
73	−188.10	−775.65	11.98	−14.80	721.36	−129.55
74	−192.27	−874.76	11.20	−16.24	825.90	−137.54
75	−211.99	−645.02	15.73	−18.10	583.17	−146.68
76	−174.81	−408.81	18.24	−17.58	376.42	−143.04
77	−187.63	−114.17	10.83	−13.79	66.19	−135.78
78	−159.39	263.74	13.41	−15.73	−274.68	−144.89
79	−110.04	646.18	19.85	−16.30	−618.51	−140.16
80	−201.40	−427.22	12.27	−15.67	376.28	−145.86
81	−152.12	236.52	15.06	−15.36	−248.31	−138.58
82	−143.98	−102.18	16.34	−16.00	97.24	−138.60
83	−128.85	−181.38	10.95	−13.70	219.61	−163.86
84	−152.96	135.82	13.08	−14.34	−148.77	−137.28
85	−130.42	−315.31	22.55	−13.98	322.40	−144.89
86	−174.81	−408.81	18.24	−17.58	376.42	−143.04
87	−147.97	−143.61	17.54	−13.86	130.80	−137.57
88	−167.19	−501.46	14.16	−15.30	492.08	−155.73
89	−157.83	−285.45	11.38	−13.67	274.63	−144.68
90	−143.95	84.55	14.09	−11.88	−89.30	−140.87
91	−143.02	364.34	9.26	−12.85	−356.79	−146.62
92	−109.29	568.14	8.16	−13.69	−516.02	−155.45
93	−108.63	149.62	12.97	−10.92	−131.99	−128.06
94	−126.76	−66.99	14.89	−12.05	75.85	−137.78
95	−152.56	−423.48	16.29	−12.36	410.52	−143.53
96	−134.54	216.66	7.79	−15.13	−192.11	−151.74
97	−94.86	438.80	19.30	−14.14	−395.24	−143.22
98	−177.45	−770.10	13.85	−13.21	732.32	−140.26
99	−172.92	−544.26	15.79	−14.79	507.75	−137.26
100	−150.62	93.11	15.71	−15.16	−93.17	−150.29
average	−152.57	−175.05	15.68	−14.99	169.56	−146.80
min	−94.86	646.18	27.87	−10.92	825.90	−106.62
max	−211.99	−875.66	0.70	−19.01	−618.51	−171.95

2.6. "Molecular Dynamic Simulation". In order to assess the stability of daidzein in the bound form with *Mtb* DNA GyrB and to look into the interactions between ligands and protein complexes in dynamic behavior, molecular dynamic simulation was carried out. To investigate the daidzein-DNA GyrB complex conformational stability, we simulated the systems for up to 100 ns. A 100 ns timeframe was used in this investigation, which is sufficient time for the configurations of *Mtb* DNA GyrB C atoms in complex with daidzein. During dynamics analysis, the protein backbone's RMSD values were used to determine the stability of the daidzein-DNA GyrB complex, as shown in Figure 7. It is expected that the lower the RMSD value during the simulation, the more stable the daidzein-DNA GyrB complex.[36]

Due to equilibration, the ligand RMSDs first fluctuated with a value of 1.5 Å at 5 ns; however, it was within the range of 1.5 to 3 Å till 70 ns of the simulation time (Figure 7A). Drastic change in the RMSD of the ligand has been observed between 80 and 90 ns due to the flipping of the chromen-4-one ring (Figure 8). Over the course of the simulation, which lasted 100 ns, it was noted that the protein had minor RMSD changes, with values between 2 and 2.5 Å. Figure 7B displays the RMSF values of DNA GyrB's backbone residue. The peaks in these graphs represent the variation of each amino acid residue during the simulation. It implies that higher RMSF values correspond to greater residue flexibility, whereas lower RMSF values correspond to less residue flexibility and greater system stability. The loop area is shown in white on the RMSF map, while secondary structural elements like the α-helical and β-

https://doi.org/10.1021/acsomega.3c00684
ACS Omega 2023, 8, 16228−16240

strand regions are shown with red and blue backgrounds, respectively (Figure 7B). The results in Figure 7B indicate that the active site residue varied minimally resulting in firm confinement of daidzein in the DNA GyrB domain.[37]

The RMSF plot of the daidzein-GyrB complex (Figure 7B) revealed that the protein backbone residues in the catalytic domain exhibited RMSF values ranging from 0.3 to 3.0, with a notable difference in the C- and N-terminal regions compared to other regions of the protein. During the 100 ns time of simulation, daidzein was identified to contact 17 amino acids of the *Mtb* DNA GyrB protein, including ALA126, ARG128, PTR129, ASP89, ALA90, SER91, ASP94, LYS44, ASP461, SER462, ARG482, GLY483, LYS484, LYS498, ASN499, THR500, and GLU501. All of these interacting residues have RMSF values of less than 3.0 (Figure 7B). Protein-ligand interactions revealed that the Arg128 residue had 72% hydrogen bond interactions with the daidzein's carbonyl oxygen (C═O). At the third position of the chromen-4-one, Arg128 and Arg482 were forming a $\pi-\pi$ interaction with the phenyl ring. The 4-hydroxy group of the phenyl ring forms a water-mediated hydrogen bond interaction with ASP461 and SER462 and a direct hydrogen bond interaction with PTR 129 (Figure 7C,D).

We also looked into the ligand properties of the simulated daidzein, and we discovered that its RMSD was under 0.9. The ligand's extendibility is measured by the "*Radius of Gyration*", and throughout the 100 ns timeframe of simulation time, it was observed to be below 3.72 Å. No intramolecular hydrogen bonding has been observed in the ligand. "*Molecular Surface Area*" indicates the "*van der Waals surface area*", and it was observed to be 238 Å^2, denoting the polar nature of the ligand. The surface of a molecule that is accessible by water molecules is known as the solvent accessible surface area (SASA), and it was found to be between 280 and 320 Å^2.

A molecule's "*Polar Surface Area (PSA)*" is the SASA due to oxygen and nitrogen. It was 156−160 Å^2 for daidzein due to the presence of 4 oxygen (Figure 7E). The postdynamic MMGBSA analysis of the daidzein-GyrB complex was performed at each nanosecond for 100 frames of the MD simulation of daidzein. Daidzein showed an average post-dynamic binding free energy of −152.57 kcal/mol (Table 3). .

Dynamic cross-correlation matrices (DCCMs) are widely used to calculate the dynamic correlation between the Cα atoms of each amino acid in a protein, and they provide some information about the relative motion of proteins in a large-scale range.[38] In order to observe the difference in the conformational movement of GyrB caused by the inhibition of daidzein, DCCM analysis was performed on the skeleton atoms of GyrB (Figure 9).

The DCCM analysis was utilized to comprehend the correlations of residue movements in various domains. The blue color regions in the DCCM plot indicate the correlated motion of the specific residue, whereas the red color region denotes the anticorrelated motions of the residue.[45] The deeper the color intensity of the blue or red, the stronger the positive or negative correlation. The RMSF graph and the DCCM graph are interlinked with each other, and one can easily draw the conclusion about the increase and decrease in RMSF from the DCCM (positive and negative correlations of amino acid residue) (Figures 7B and 9).[39] The residues from 1 to 450 were in the positive correlation movement (D1 domain), and similarly, in the RMSF graph, they have an RMSF value less than 3.0 Å. From the 450 to 500 residue

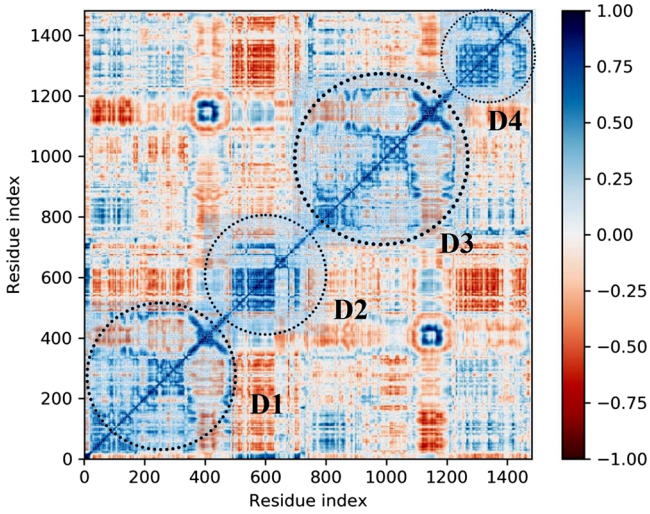

Figure 9. DCCM analysis of daidzein (blue color: positive correlation; red color: negative correlation).

index, there was a mixed patch of blue and red regions, resulting in an increase in the RMSF value (3.0 to 4.2 Å) in the RMSF graph (Figures 7B and 9). There was a dark blue color from the residue index 500 to 700, indicating positive correlation of these residues. There was a mixed patch of bluish-red color in the 700−750 residue index that resulted in an increase in RMSF of these residues up to 5 Å (Figures 7B and 9). The D3 domain spans from 800 to 1200 residue index. There was a slight increase in RMSF around the 1250 residue index in the RMSF graph due to the decrease in positive correlation of these amino acids. From the 1250 to 1450 residue index, a dark bluish color indicates the positive correlation. The comparison among the domains indicated that D2 and D4 domains were in anticorrelated motion with each other (Figures 7B and 9). In order to learn more about the conformational states of daidzein-GyrB, PCA analysis was carried out utilizing the 100 ns MD simulation trajectory. This method assisted in determining the Cα atoms' overall combined motion, which was shown by the "*eigenvectors of the covariance matrix*" and supported by its eigenvalues.[38,39] Typically, the frequency of the eigenvectors with high eigenvalues could be used to determine the protein's overall coordinated motion.[38,39] As depicted in Figure 10, the first 20 PC values of the daidzein-GyrB system accounted for 25.045% of the total variation in the 100 ns trajectory. Most of the variance in the initial protein conformational space distribution was captured by the first two eigenvectors (PC1 and PC2). As a result, the trajectories of the first two eigenvectors (PC1 and PC2) were projected onto the two-dimensional space image in order to study the conformation changes of the daidzein-GyrB system. Figure 10 depicts the scatter plot of PC1 vs PC2. A cluster of PC1 and PC2 was dispersed parallel to each side of the diagonal line, as illustrated in Figure 10, demonstrating the stability of the conformation.[46]

2.7. Frontier Molecular Orbital and Molecular Electrostatic Potential Analysis. To better understand the chemical reactivity of the NPs in various forms, "*the frontier molecular orbitals (HOMO and LUMO)*" have been studied. The "*HOMO and LUMO energies*" have an impact on how the molecule interacts with other species and help us in understanding its "*chemical reactivity and kinetic stability*", Most frequently, HOMO is employed as an "*electron donor*",

https://doi.org/10.1021/acsomega.3c00684
ACS Omega 2023, 8, 16228−16240

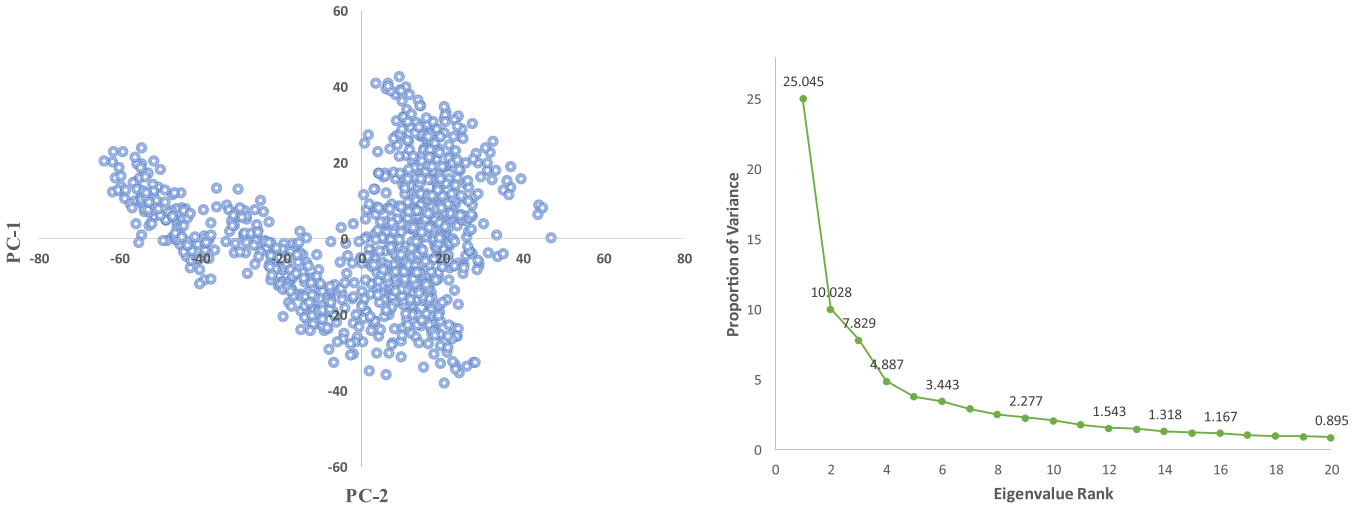

Figure 10. Trajectories for the daidzein-GyrB complex are projected into PC1 and PC2.

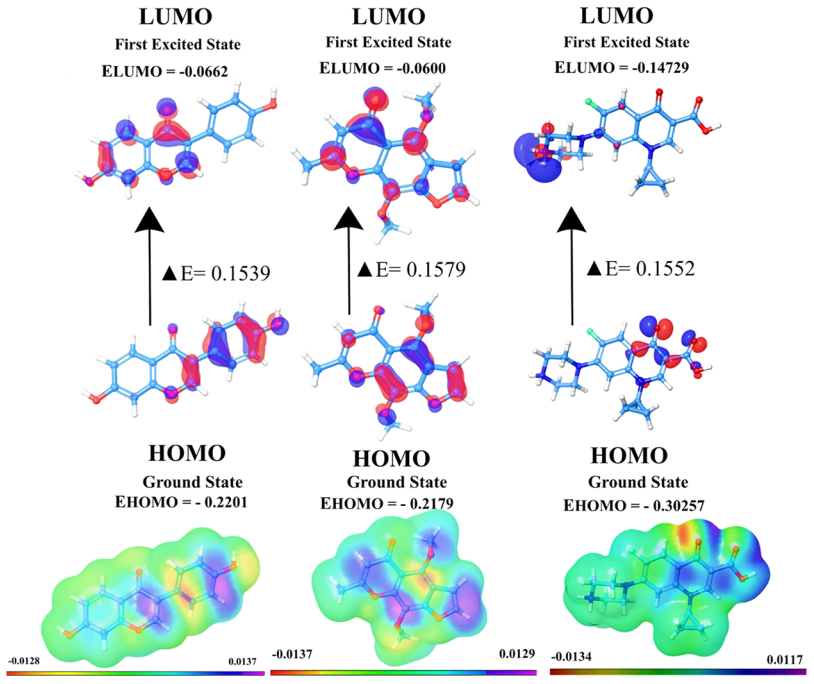

Figure 11. DFT-based HOMO, LUMO and MESP calculation of daidzein and khellin and ciprofloxacin.

while LUMO is used as an "*electron acceptor*".[36,40,41] In addition, the "*HOMO-LUMO energy gap (E)*" is a useful tool for estimating the reactivity and stability of a molecule. The harder and more stable molecule has a larger energy difference between the HOMO and LUMO and is consequently less reactive. The possibility of charge-transfer interaction within the molecules increases with decreasing LUMO-HOMO differential.

Functionally, compounds having a high capacity for electron transfer may bind to proteins more readily by interacting more effectively with the target protein structure.[42] The "*HOMO-LUMO energy gap (ΔE)*" of daidzein (Δ*E* = 0.1539) was lower compared to khellin (Δ*E* = 0.1579), and hence it was found to be the most active in the study (Figure 11).

The "*molecular electrostatic potential (MESP)*" surface provides details of charge distribution and estimates the regions of reactive compounds that could be attacked by electrophiles and nucleophiles. MESP diagrams are helpful for showing how, depending on color gradation, they appear as positive, negative, or neutral electrostatic potential zones of a compound. Increases in the molecular electrostatic potential were color coded as red, orange, yellow, green, and blue.[43,44] The most negative part of a molecule is its red region, which also makes it more susceptible to electrophilic attack. Contrarily, the most vulnerable area to a nucleophilic attack is the blue zone, which is the most positive region (Figure 11). The negative electrostatic potential is shown by the red areas on these maps, but they also represent the area where the electron density is greater than the nucleus throughout the entire molecule, rendering it vulnerable to chemical reactions.[44] The blue regions are reactively unstable and have partial positive charges. Green indicates areas that are almost neutral, whereas yellow indicates areas with less electrons.[45] Around daidzein, the highest color density was

https://doi.org/10.1021/acsomega.3c00684
ACS Omega 2023, 8, 16228−16240

seen, and it was a neutral green color brought on by aromatic hydrocarbons.

A slight reddish-yellow color has been observed around the OH, C═O, and chromen ring's oxygen due to the electron-rich nature of these atoms. These reactivity centers will enable the chemical to engage in interactions with charged systems in physiological organisms, producing the necessary bioactivity (Figure 11). As per the MESP results, daidzein formed hydrogen bond interaction via the 7-hydroxy group present on chromen-4-one of daidzein with ASP 94. The carbonyl oxygen at the C-4 position of the chromen-4-one ring established the hydrogen bond interaction with Arg 128. The 4-hydroxy group of 4-hydroxyphenyl formed two hydrogen bond interactions, one with Gly 483 and the other with PTR 129 (Figures 11 and 4).

3. CONCLUSIONS

In conclusion, we have screened 16 NPs containing the flavonoid, isoflavonoid, chromone, coumarin, chalcone, anthraquinone, pyridine, quinoline, piperidine, and piperazine core as antimycobacterial agents. Among them, daidzein and khellin were found to be effective against the $H_{37}Rv$ strain of *M. tuberculosis* with an MIC of 25 μg/mL. The cytotoxicity study of these two NPs showed that they are less toxic for the vero cell line (IC_{50} = > 150 μg/mL). Except for garcinone B (Figure 2), both daidzein and khellin showed significant antimycobacterial activity when compared with the previously reported isoflavonoid and furanochromone (Figures 1 and 2). To get insight into the molecular mechanism of action of the NP's, DNA gyrase inhibition was measured, and both daidzein and khellin inhibited the DNA gyrase enzyme with IC_{50} values of 0.042 μg/mL and 0.822 μg/mL, respectively, compared to ciprofloxacin with IC_{50} of 0.018 μg/mL. Both the compounds were characterized by TLC (R_f calculation), melting point, ATR-IR, ^{1}H NMR and ^{13}C NMR spectroscopy and by mass spectrometry technique. Daidzein and khellin were docked into the DNA GyrB domain of *M. tuberculosis* obtained from the protein data bank (PDB ID: 5BS8). Both the compounds showed crucial hydrogen bonding with Arg 128 amino acid. The MD simulation study of daidzein showed that it remains stable in the DNA GyrB domain for 100 ns time, and the stability of the ligand was further confirmed by the DCCM and PCA analysis. Further, DFT-based HOMO, LUMO, and MESP explained the reactivity of daidzein and khellin. As a future perspective, further semisynthetic analogues of daidzein and khellin may lead to the development of potent antimycobacterial compounds.

4. EXPERIMENTAL SECTION

4.1. General. The IR spectra were recorded using ATR-FTIR, Affinity 1 s, Shimadzu, and the reported wave numbers are given in cm^{-1}. The ^{1}H and ^{13}C NMR spectra were assessed using a "*Brüker Avance New 500 MHz spectrometer*" in DMSO as the solvent and TMS as the internal reference standard.[46]

4.2. In Vitro *Mtb* MABA Assay. The MIC of the NPs was determined using the MABA method as described by Krishna et al.[47] using *Mtb* $H_{37}Rv$ strain.

4.3. DNA Gyrase Inhibitory Activity. The NPs were tested for their ability to inhibit DNA gyrase from *E. coli*. The assay was carried out using established protocols obtained from TopoGEN, Inc. (Buena Vista, Colorado, USA).[48] The detailed procedure is given in our previously published paper.[49] In brief, various concentrations of test compounds were prepared in DMSO and added to the reaction mixture, followed by the addition of two units of the DNA gyrase enzyme. Ciprofloxacin was tested in the same experiment as the standard for comparison. The positive control was the relaxed pBR322 DNA+ DNA gyrase enzyme (without the test compound). The negative control was relaxed pBR322 DNA without the DNA gyrase enzyme.[49]

4.4. Docking Study. The phytocompounds were docked in the DNA GyrB domain of *M. tuberculosis* retrieved from protein data bank (PDB ID: 5BS8). The protein was first processed with Schrödinger Suite 2012's Protein Preparation Wizard. There is overlap of the EF and GH chain, both of which are of DNA double-helical strand. Hence, we reserved the GH chain containing moxifloxacin and deleted the EF. The protein and ligands were optimized using the OPLS force field. The grid was generated around the cocrystallized ligand moxifloxacin.[50−52] The binding free energy between the NPs and DNA GyrB domain was calculated by the MMGBSA approach.[53]

4.5. MD Simulation. The MD simulation was used to investigate the thermodynamic stability of the docked daidzein-DNA GyrB complex.[54,55] The daidzein-DNA GyrB complex was solvated using the "*single point charge*" water model. The system was neutralized by using Desmond's system builder to add the Na+ and Cl$^-$ counterions to an orthorhombic cell.[54,55] The system was relaxed using a six-stage NPT protocol before the MD simulation.[54,55] The daidzein-DNA GyrB complex was further submitted for 100 ns MD simulation study. The stability of the complex was analyzed by evaluating the MD trajectories utilizing the "*Desmond's Simulation Interaction Diagram*".[54,55] The binding free energy of the daidzein-DNA GyrB complex was calculated using the Python script "*thermal mmgbsa. py*".[54,55]

4.6. DFT/B3LYP Calculations. The B3LYP/6-311** basis set was used to optimize the geometry and calculate the DFT of the NPs. The quantum chemical properties of the NPs, such as LUMO, HOMO, and MESP, were further investigated using the previously described procedure.[56,57]

■ ASSOCIATED CONTENT

Supporting Information

The Supporting Information is available free of charge at https://pubs.acs.org/doi/10.1021/acsomega.3c00684.

Spectral data of the study (PDF)

■ AUTHOR INFORMATION

Corresponding Author

Harun Patel − *Division of Computer-Aided Drug Design, Department of Pharmaceutical Chemistry, R. C. Patel Institute of Pharmaceutical Education and Research, Dhule 425405 Maharashtra, India;* orcid.org/0000-0003-0920-1266; Email: hpatel_38@yahoo.com

Authors

Vilas R. Jagatap − *Division of Computer-Aided Drug Design, Department of Pharmaceutical Chemistry, R. C. Patel Institute of Pharmaceutical Education and Research, Dhule 425405 Maharashtra, India*

Iqrar Ahmad − *Division of Computer-Aided Drug Design, Department of Pharmaceutical Chemistry, R. C. Patel*

https://doi.org/10.1021/acsomega.3c00684
ACS Omega 2023, 8, 16228−16240

Institute of Pharmaceutical Education and Research, Dhule 425405 Maharashtra, India

Dharmarajan Sriram − *Department of Pharmacy, Birla Institute of Technology and Science-Pilani, Hyderabad 500078, India*

Jyothi Kumari − *Department of Pharmacy, Birla Institute of Technology and Science-Pilani, Hyderabad 500078, India*

Darko Kwabena Adu − *Department of Pharmaceutical Chemistry, Discipline of Pharmaceutical Sciences, College of Health Sciences, University of KwaZulu-Natal (Westville), Durban 4000, South Africa*

Blessing Wisdom Ike − *Department of Pharmaceutical Chemistry, Discipline of Pharmaceutical Sciences, College of Health Sciences, University of KwaZulu-Natal (Westville), Durban 4000, South Africa*

Meenu Ghai − *Discipline of Genetics, School of Life Sciences, University of KwaZulu-Natal, Durban 4000, South Africa*

Siddique Akber Ansari − *Department of Pharmaceutical Chemistry, College of Pharmacy, King Saud University, Riyadh 11451, Saudi Arabia*

Irfan Aamer Ansari − *Department of Drug Science and Technology, University of Turin, Turin 10124, Italy*

Priscille Ornella Mefotso Wetchoua − *Department of Pharmaceutical Chemistry, Discipline of Pharmaceutical Sciences, College of Health Sciences, University of KwaZulu-Natal (Westville), Durban 4000, South Africa*

Rajshekhar Karpoormath − *Department of Pharmaceutical Chemistry, Discipline of Pharmaceutical Sciences, College of Health Sciences, University of KwaZulu-Natal (Westville), Durban 4000, South Africa;* orcid.org/0000-0002-7814-0965

Complete contact information is available at: https://pubs.acs.org/10.1021/acsomega.3c00684

Notes

The authors declare no competing financial interest.

■ ACKNOWLEDGMENTS

We are thankful to the Researchers Supporting Project (RSPD2023R744), King Saud University, Riyadh, Saudi Arabia. We are also thankful to the Jamia Hamdard-New Delhi in assisting molecular modeling facilities.

■ REFERENCES

(1) Shetye, G. S.; Franzblau, S. G.; Cho, S. New tuberculosis drug targets, their inhibitors, and potential therapeutic impact. *Transl. Res.* **2020**, *220*, 68−97.

(2) Hu, Y. Q.; Zhang, S.; Zhao, F.; Gao, C.; Feng, L. S.; Lv, Z. S.; Xu, Z.; Wu, X. Isoniazid derivatives and their anti-tubercular activity. *Eur. J. Med. Chem.* **2017**, *133*, 255−267.

(3) Girase, P. S.; Dhawan, S.; Kumar, V.; Shinde, S. R.; Palkar, M. B.; Karpoormath, R. An appraisal of anti-mycobacterial activity with structure-activity relationship of Piperazine and its analogues: A review. *Eur. J. Med. Chem.* **2020**, *210*, No. 112967.

(4) Mishra, S. K.; Tripathi, G.; Kishore, N.; Singh, R. K.; Singh, A.; Tiwari, V. K. Drug development against tuberculosis: Impact of alkaloids. *Eur. J. Med. Chem.* **2017**, *137*, 504−544.

(5) Okunade, A. L.; Elvin-Lewis, M. P.; Lewis, W. H. Natural anti-mycobacterial metabolites: current status. *Phytochemistry* **2004**, *65*, 1017−1032.

(6) Kishore, N.; Mishra, B. B.; Tripathi, V.; Tiwari, V. K. Alkaloids as potential anti-tubercular agents. *Fitoterapia* **2009**, *80*, 149−163.

(7) Hou, X. M.; Wang, C. Y.; Gerwick, W. H.; Shao, C. L. Marine natural products as potential anti-tubercular agents. *Eur. J. Med. Chem.* **2019**, *165*, 273−292.

(8) Monga, A.; Sharma, A. Natural products encompassing antituberculosis activities. *Stud. Nat. Prod. Chem.* **2020**, *64*, 263−301.

(9) Vasava, M. S.; Nair, S. G.; Rathwa, S. K.; Patel, D. B.; Patel, H. D. Development of new drug-regimens against multidrug-resistant tuberculosis. *Indian J. Tuberc.* **2019**, *66*, 12−19.

(10) https://www.who.int/news-room/fact-sheets/detail/tuberculosis.

(11) Chraibi, M.; Farah, A.; Lebrazi, S.; El Amine, O.; Houssaini, M. I.; Fikri-Benbrahim, K. Anti-mycobacterial natural products from Moroccan medicinal plants: Chemical composition, bacteriostatic and bactericidal profile of Thymus satureioides and Mentha pulegium essential oils. *Asian Pac. J. Trop. Biomed.* **2016**, *6*, 836−840.

(12) Luo, X.; Pires, D.; Aínsa, J. A.; Gracia, B.; Mulhovo, S.; Duarte, A.; Anes, E.; Ferreira, M. J. U. Anti-mycobacterial evaluation and preliminary phytochemical investigation of selected medicinal plants traditionally used in Mozambique. *J. Ethnopharmacol.* **2011**, *137*, 114−120.

(13) Liu, Y.; Matsumoto, M.; Ishida, H.; Ohguro, K.; Yoshitake, M.; Gupta, R.; Geiter, L.; Hafkin, J. Delamanid: From discovery to its use for pulmonary multidrug-resistant tuberculosis (MDR-TB). *Tuberculosis* **2018**, *111*, 20−30.

(14) Choi, W. H. Evaluation of anti-tubercular activity of linolenic acid and conjugated-linoleic acid as effective inhibitors against *Mycobacterium tuberculosis*. *Asian Pac. J. Trop. Med.* **2016**, *9*, 125−129.

(15) Dong, M.; Pfeiffer, B.; Altmann, K. H. Recent developments in natural product-based drug discovery for tuberculosis. *Drug Discovery Today* **2017**, *22*, 585−591.

(16) Newman, D. J.; Cragg, G. M. Natural Products as Sources of New Drugs from 1981 to 2014. *J. Nat. Prod.* **2016**, *79*, 629−661.

(17) Farah, S. I.; Abdelrahman, A. A.; North, E. J.; Chauhan, H. Opportunities and Challenges for Natural Products as Novel Antituberculosis Agents. *Assay Drug Dev. Technol.* **2015**, *14*, 29−38.

(18) Newton, S. M.; Lau, C.; Wright, C. W. A review of anti-mycobacterial natural products. *Phytoth. Res.* **2000**, *14*, 303−322.

(19) Keri, R. S.; Sasidhar, B. S.; Nagaraja, B. M.; Santos, M. A. Recent progress in the drug development of coumarin derivatives as potent antituberculosis agents. *Eur. J. Med. Chem.* **2015**, *100*, 257−269.

(20) Coronado-Aceves, E. W.; Gigliarelli, G.; Garibay-Escobar, A.; Zepeda, R. E. R.; Curini, M.; López Cervantes, J.; Inés Espitia Pinzón, C. I.; Superchi, S.; Vergura, S.; Marcotullio, M. C. New Isoflavonoids from the extract of Rhynchosia precatoria (Humb. & Bonpl. ex Willd.) DC. and their anti-mycobacterial activity. *J. Ethnopharmacol.* **2017**, *206*, 92−100.

(21) Songsiang, U.; Wanich, S.; Pitchuanchom, S.; Netsopa, S.; Uanporn, K.; Yenja, C. Bioactive constituents from the stems of Dalbergia parviflora. *Fitoterapia* **2009**, *80*, 427−431.

(22) Chokchaisiri, R.; Suaisom, C.; Sriphota, S.; Chindaduang, A.; Chuprajob, T.; Suksamrarn, A. Bioactive Flavonoids of the Flowers of Butea monosperma. *Chem. Pharm. Bull.* **2009**, *57*, 428−432.

(23) Chen, L. W.; Cheng, M. J.; Peng, C. F.; Chen, I. S. Secondary metabolites and anti-mycobacterial activities from the roots of Ficus nervosa. *Chem. Biodiversity* **2010**, *7*, 1814−1821.

(24) Wu, M. C.; Peng, C. F.; Chen, I. S.; Tsai, I. L. Antitubercular chromones and flavonoids from Pisonia aculeata. *J. Nat. Prod.* **2011**, *74*, 976−982.

(25) Tuntiwachwuttikul, P.; Phansa, P.; Pootaeng On, Y.; Taylor, W. C. Chromones from the branches of Harrisonia perforate. *Chem. Pharm. Bull.* **2006**, *54*, 44−47.

(26) Skusamrarn, S.; Suwannapoch, N.; Phakhodee, W.; Thanuhiranlert, J.; Ratananukul, P. Anti-mycobacterial activity of prenylated xanthones from the fruits of Garcinia mangostana. *Chem. Pharm. Bull.* **2003**, *51*, 857−859.

(27) Rabaan, A. A.; Alhumaid, S.; Albayat, H.; Alsaeed, M.; Alofi, F. S.; Al-Howaidi, M. H.; Turkistani, S. A.; Alhajri, S. M.; Alahmed, H. E.; Alzahrani, A. B.; Mashraqi, M. M.; Alwarthan, S. Promising Anti-

mycobacterial Activities of Flavonoids against Mycobacterium sp Drug Targets: A Comprehensive Review. *Molecules* **2022**, *27*, 5335.
(28) Reddy, D. S.; Kongot, M.; Kumar, A. Coumarin hybrid derivatives as promising leads to treat tuberculosis: Recent developments and critical aspects of structural design to exhibit antitubercular activity. *Tuberculosis* **2021**, *127*, No. 102050.
(29) Rodríguez-Silva, C. N.; Prokopczyk, I. M.; Dos Santos, J. L. The Medicinal Chemistry of Chalcones as Anti-Mycobacterium tuberculosis Agents. *Mini Rev. Med. Chem.* **2022**, *22*, 2068−2080.
(30) Cui, Y.; Chen, L. J.; Huang, T.; Ying, J. Q.; Li, J. The pharmacology, toxicology and therapeutic potential of anthraquinone derivative emodin. *Chin. J. Nat. Med.* **2020**, *18*, 425−435.
(31) Villamizar-Mogotocoro, A. F.; Vargas-Méndez, L. Y.; Kouznetsov, V. V. Pyridine and quinoline molecules as crucial protagonists in the never-stopping discovery of new agents against tuberculosis. *Eur. J. Pharm. Sci.* **2020**, *151*, No. 105374.
(32) Swain; Pati, S.; Hussain, T. Quinoline heterocyclic containing plant and marine candidates against drug-resistant Mycobacterium tuberculosis: A systematic drug-ability investigation. *Eur. J. Med. Chem.* **2022**, *232*, No. 114173.
(33) Xu, Y.; Liang, B.; Kong, C.; Sun, Z. Traditional Medicinal Plants as a Source of Antituberculosis Drugs: A System Review. *Biomed. Res. Int.* **2021**, *2021*, No. 9910365.
(34) Chaudhari, K.; Surana, S.; Jain, P.; Patel, H. M. Mycobacterium Tuberculosis (*MTB*) GyrB inhibitors: An attractive approach for developing novel drugs against TB. *Eur. J. Med. Chem.* **2016**, *124*, 160−185.
(35) Karunanidhi, S.; Chandrasekaran, B.; Karpoormath, R.; Patel, H. M.; Kayamba, F.; Merugu, S. R.; Kumar, V.; Dhawan, S.; Kushwaha, B.; Mahlalela, M. C. Novel thiomorpholine tethered isatin hydrazones as potential inhibitors of resistant Mycobacterium tuberculosis. *Bioorg. Chem.* **2021**, *115*, No. 105133.
(36) Zrieq, R.; Ahmad, I.; Snoussi, M.; Noumi, E.; Iriti, M.; Algahtani, F. D.; Patel, H.; Saeed, M.; Tasleem, M.; Sulaiman, S.; Aouadi, K. Tomatidine and patchouli alcohol as inhibitors of SARS-CoV-2 enzymes (3CLpro, PLpro and NSP15) by molecular docking and molecular dynamics simulations. *Int. J. Mol. Sci.* **2021**, *22*, 10693.
(37) Malani, A.; Atul, M.; Jahnvi, M.; Iqrar, A.; Harun, P.; Nisheeth, D. Synthesis, molecular docking, DFT study, and in vitro antimicrobial activity of some 4-(biphenyl-4-yl)-1, 4-dihydropyridine and 4-(biphenyl-4-yl) pyridine derivatives. *J. Biochem. Mol. Toxicol.* **2021**, *35*, No. e22903.
(38) Li, W. Y.; Wei, H. Y.; Sun, Y. Z.; Zhou, H.; Ma, Y.; Wang, R. L. Exploring the effect of E76K mutation on SHP2 cause gain-of-function activity by a molecular dynamics study. *J. Cell. Biochem.* **2018**, *119*, 9941−9956.
(39) Du, S.; Yang, B.; Wang, X.; Li, W. Y.; Lu, X. H.; Zheng, Z. H.; Ma, Y.; Wang, R. L. Identification of potential leukocyte antigen-related protein (PTP-LAR) inhibitors through 3D QSAR pharmacophore-based virtual screening and molecular dynamics simulation. *J. Biomol. Struct. Dyn.* **2020**, *38*, 4232−4245.
(40) Ghosh, S.; Das, S.; Ahmad, I.; Patel, H. In silico validation of anti-viral drugs obtained from marine sources as a potential target against SARS-CoV-2 Mpro. *J. Indian Chem. Soc.* **2021**, *98*, No. 100272.
(41) Srivastava, R.; Gupta, S. K.; Naaz, F.; Gupta, P. S. S.; Yadav, M.; Singh, V. K.; Singh, A.; Rana, M. K.; Gupta, S. K.; Schols, D.; Singh, R. K. Alkylated benzimidazoles: Design, synthesis, docking, DFT analysis, ADMET property, molecular dynamics and activity against HIV and YFV. *Comput. Biol. Chem.* **2020**, *89*, No. 107400.
(42) Milanović, Ž. B.; Marković, Z. S.; Dimić, D. S.; Klisurić, O. R.; Radojević, I. D.; Šeklić, D. S.; Živanović, M. N.; Marković, J. D.; Radulović, M.; Avdović, E. H. Synthesis, structural characterization, biological activity and molecular docking study of 4, 7-dihydroxycoumarin modified by aminophenol derivatives. *C. R. Chim.* **2021**, *24*, 215−232.
(43) Mary, Y. S.; Yalcin, G.; Mary, Y. S.; Resmi, K. S.; Thomas, R.; Önkol, T.; Kasap, E. N.; Yildiz, I. Spectroscopic, quantum mechanical studies, ligand protein interactions and photovoltaic efficiency modeling of some bioactive benzothiazolinone acetamide analogs. *Chem. Pap.* **2020**, *74*, 1957−1964.
(44) Pawara, R.; Ahmad, I.; Nayak, D.; Belamkar, S.; Surana, S.; Kundu, C. N.; Patil, C.; Patel, H. Design and synthesis of the novel, selective WZ4002 analogue as EGFR-L858R/T790M tyrosine kinase inhibitors for targeted drug therapy in non-small-cell lung cancer (NSCLC). *J. Mol. Struct.* **2022**, *1254*, No. 132313.
(45) Ahmad, I.; Shaikh, M.; Surana, S.; Ghosh, A.; Patel, H. p38α MAP kinase inhibitors to overcome EGFR tertiary C797S point mutation associated with osimertinib in non-small cell lung cancer (NSCLC): emergence of fourth-generation EGFR inhibitor. *J. Biomol. Struct. Dyn.* **2022**, *40*, 3046−3059.
(46) Ahmad, I.; Pawara, R. H.; Girase, R. T.; Pathan, A. Y.; Jagatap, V. R.; Desai, N.; Ayipo, Y. O.; Surana, S. J.; Patel, H. Synthesis, Molecular Modeling Study, and Quantum-Chemical-Based Investigations of Isoindoline-1,3-diones as Anti-mycobacterial Agents. *ACS Omega* **2022**, *7*, 21820−21844.
(47) Krishna, V. S.; Zheng, S.; Rekha, E. M.; Guddat, L. W.; Sriram, D. Discovery and evaluation of novel *Mycobacterium tuberculosis*ketol-acid reductoisomerase inhibitors as therapeutic drug leads. *J. Comput.-Aided Mol. Des.* **2019**, *33*, 357−366.
(48) https://topogen.com/product/e-coli-dna-gyrase-drug-screening-kit/ (Accessed March 15, 2023).
(49) Shinde, S. R.; Inamdar, S. N.; Shinde, M.; Pawar, C.; Kushwaha, B.; Obakachi, V. A.; Kajee, A.; Chauhan, R.; Karpoormath, R. Discovery of oxazoline-triazole based hybrid molecules as DNA gyrase inhibitors: A new class of potential Anti-tubercular agents. *J. Mol. Struct.* **2023**, *1273*, No. 134243.
(50) Aubry, A.; Pan, X. S.; Fisher, L. M.; Jarlier, V.; Cambau, E. Mycobacterium tuberculosis DNA gyrase: interaction with quinolones and correlation with anti-mycobacterial drug activity. *Antimicrob. Agents Chemother.* **2004**, *48*, 1281−1288.
(51) Patel, H.; Sonawane, Y.; Jagtap, R.; Dhangar, K.; Thapliyal, N.; Surana, S.; Noolvi, M.; Shaikh, M. S.; Rane, R. A.; Karpoormath, R. Structural insight of glitazone for hepato-toxicity: Resolving mystery by PASS. *Bioorg. Med. Chem. Lett.* **2015**, *25*, 1938−1946.
(52) Patel, H. M.; Palkar, M.; Karpoormath, R. Exploring MDR-TB Inhibitory Potential of 4-Aminoquinazolines as Mycobacterium tuberculosis N-Acetylglucosamine-1-Phosphate Uridyltransferase (GlmU*MTB*) Inhibitors. *Chem. Biodiversity* **2020**, *17*, No. e2000237.
(53) Girase, R.; Ahmad, I.; Pawara, R.; Patel, H. Optimizing cardio, hepato and phospholipidosis toxicity of the Bedaquiline by chemo-informatics and molecular modelling approach. *SAR QSAR Environ. Res.* **2022**, *33*, 215−235.
(54) Ahmad, I.; Jadhav, H.; Shinde, Y.; Jagtap, V.; Girase, R.; Patel, H. Optimizing Bedaquiline for cardiotoxicity by structure based virtual screening, DFT analysis and molecular dynamic simulation studies to identify selective MDR-TB inhibitors. *In Silico Pharmacol.* **2021**, *9*, 23.
(55) Abdelgawad, M. A.; Oh, J. M.; Parambi, D. G.; Kumar, S.; Musa, A.; Ghoneim, M. M.; Nayl, A. A.; El-Ghorab, A. H.; Ahmad, I.; Patel, H.; Kim, H. Development of bromo-and fluoro-based α, β-unsaturated ketones as highly potent MAO-B inhibitors for the treatment of Parkinson's disease. *J. Mol. Struct.* **2022**, *1266*, No. 133545.
(56) Senthil Kumar, K.; Kumaresanb, R. A DFT study on the structural, electronic properties and radical scavenging mechanisms of calycosin, glycitein, pratensein and prunetin. *Comput. Theor. Chem.* **2012**, *985*, 14−22.
(57) Son, N. T.; Thanh, D. T. M.; Van Trang, N. Flavone norartocarpetin and isoflavone 2′-hydroxygenistein: A spectroscopic study for structure, electronic property and antioxidant potential using DFT (Density functional theory). *J. Mol. Struct.* **2019**, *1193*, 76−88.

https://doi.org/10.1021/acsomega.3c00684
ACS Omega 2023, 8, 16228−16240